Control of an Aeroelastic System with Control Surface Nonlinearity

Conference Paper *in* Collection of Technical Papers - AIAA/ASME/ASCE/AHS/ASC Structures, Structural Dynamics and Materials Conference · April 2010

DOI: 10.2514/6.2010-2951

4 authors:

Daochun Li
Beihang University (BUAA)
57 PUBLICATIONS **488** CITATIONS
SEE PROFILE

Shijun Guo
Cranfield University
119 PUBLICATIONS **1,219** CITATIONS
SEE PROFILE

Jinwu Xiang
Beihang University (BUAA)
69 PUBLICATIONS **524** CITATIONS
SEE PROFILE

Natalia Di Matteo
kkk
7 PUBLICATIONS **33** CITATIONS
SEE PROFILE

51st AIAA/ASME/ASCE/AHS/ASC Structures, Structural Dynamics, and Materials Conference
 18th
12 - 15 April 2010, Orlando, Florida

AIAA 2010-2951

Control of an Aeroelastic System with Control Surface Nonlinearity

Daochun Li[1]
Beijing University of Aeronautics and Astronautics, Beijing 100083, P.R. China
Shijun Guo[2]
Aerospace Engineering, Cranfield University, Cranfield, Beds, MK43 0AL, UK
Jinwu Xiang[3]
Beijing University of Aeronautics and Astronautics, Beijing 100083, P.R. China
And
Natalia Di Matteo[4]
Aerospace Engineering, Cranfield University, Cranfield, Beds, MK43 0AL, UK

Abstract **Nonlinearities in aircraft mechanism are unavoidable, especially in the control system. Correct modeling of the nonlinearities is necessary for the aeroelastic analysis and control. In this paper, a rational polynomial (RP) approximation model is introduced based on actual measured force-deflection relation in aileron system. Numerical examples prove that the model can be used to describe both freeplay and hysteresis nonlinearities. So the switching point problem may be avoided in the numerical integration process. Then state-dependent Riccati equation method is used to derive a state feedback suboptimal control law for flutter suppression of a three degree-of-freedom typical airfoil section with RP nonlinearity in control surface. With the control law designed in this paper, the closed-loop dynamic system is solved by Runge-Kutta numerical approach. Simulation results are presented to show the efficacy of the designed control system. And the effects of RP nonlinearity on aeroelastic closed-loop responses are also investigated.**

Nomenclature

a	=	non-dimensional distance from airfoil mid-chord to elastic axis
b	=	airfoil semi-chord
$C(k)$	=	generalized Theodorsen function
c	=	non-dimensional distance from airfoil mid-chord to the control surface hinge line
c_i	=	coefficients of Wagner's function
h	=	plunge displacement
J	=	performance index of optimal problem
k	=	reduced frequency
L	=	aerodynamic lift
M_α, M_β	=	aerodynamic moment of wing-aileron and of aileron
m	=	mass of wing-aileron (per unit span)

[1] Postdoctoral researcher, School of Aeronautic Science and Engineering

[2] Senior Lecturer, Aerospace Engineering Department, AIAA Member

[3] Professor, School of Aeronautic Science and Engineering

[4] Postgraduate Student, Aerospace Engineering Department, Student Member of AIAA

m_t = total mass of wing-aileron and support blocks (per unit span)
$\mathbf{Q}$ = state coefficient matrix in performance index
r = control input coefficient in performance index
r_α = radius of gyration of wing-aileron
r_β = reduced radius of gyration of aileron
t = time
U = free stream velocity
$\mathbf{x_a}$ = vector of augmented variables
x_α = non-dimensional distance from airfoil elastic axis to center of mass
x_β = non-dimensional distance from aileron hinge line to center of mass
α = pitch angle about the elastic axis
β = aileron displacement about the hinge line
β_c = control input
δ = freeplay region
ρ = density of air
ς = damping ratio
ω = uncoupled natural frequency
ψ = velocity coefficient in rational polynomial approximation of hysteresis

I. Introduction

Due to various nonlinearities, aeroelastic systems exhibit a variety of phenomena such as limit cycle oscillation and chaotic vibration [1-3]. Flutter instability can jeopardize aircraft structure and its performance. A great deal of research activity devoted to flutter control of aeroelastic system has been accomplished. Kurdila et al. [4] gave an extensive review of nonlinear control methods for high-energy limit-cycle oscillations. Mukhopadhyay [5] presented an historical perspective on analysis and control of aeroelastic responses. In recent years, a large number of control strategies have been developed for the flutter suppression [6-14, 16, 17], such as adaptive decoupled fuzzy sliding-mode control[6], and tensor-product model-based control [7]. In Ref. 7, parameter-varying state-space model was transformed into the tensor- product model whereupon linear matrix inequality techniques in the parallel distributed compensation design framework can be executed to define controller. As an extension of Ref. 7, an observer was derived via LMI-based design to estimate the practically unmeasurable state values from the output values [8]. A multiple-input and multiple-output adaptive control law was designed via both leading and trailing edge control surfaces [9]. For the two-degree-of-freedom aeroelastic system with uncertainties, many effective adaptive control laws were designed by Singh et al. [10-14]. Mracek et al. [15] carried out a control design of the nonlinear benchmark problem using the state-dependent Riccati equation (SDRE) method. Then SDRE control technique was developed to design suboptimal control laws for nonlinear aeroelastic systems [16-17].

A state-space linear model with control input of a typical three degrees-of-freedom airfoil section was developed by Edwards et al. [18]. Conner et al. [19] successfully adapted the model to investigate the effect of structural freeplay on an open-loop system response in numerical and experimental approach. In previous research, most of the flutter control was studied with polynomial nonlinearity in pitching degree-of-freedom, and without considering any nonlinearity in the control surface [6-17]. The polynomial nonlinearity has the characteristic of differentiability whereas the system with one of freeplay and hysteresis is differentiable. Therefore some of the control law designed can't be used directly for the aeroelastic system with either freeplay or hysteresis nonlinearity.

In the current paper, a RP approximate model is first introduced to replace both freeplay and hysteresis nonlinearities. And then the nonlinear model has been considered in the design of a state feedback control law for flutter suppression. With the control law designed, the effect of control surface RP nonlinearity on the aeroelastic response and flutter suppression have been investigated.

II. Modeling of Nonlinearities in aeroelastic system

Structural nonlinearities in aeroelastic system were summarized into three types: cubic, freeplay, and hysteresis as early as 1950s [20, 21]. From then, many research works have focused on the three types of nonlinearities, especially on the freeplay and cubic nonlinearities. However, actual nonlinear force-deflection relationships measured from aircraft structure are not exactly the same with the three nonlinearities. Two of the examples are given in Fig. 1, in which both of the two figures show the nonlinearity in aileron system [22, 23]. Figure 1.a describes a nonlinear relationship of a coupling of cubic and freeplay, and Fig. 1.b shows unsymmetrical hysteresis circles with different aileron hinge angles.

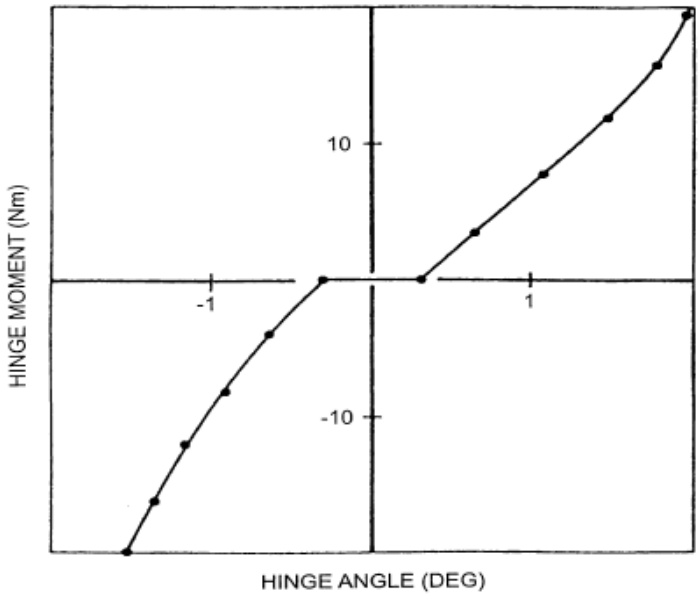

a)

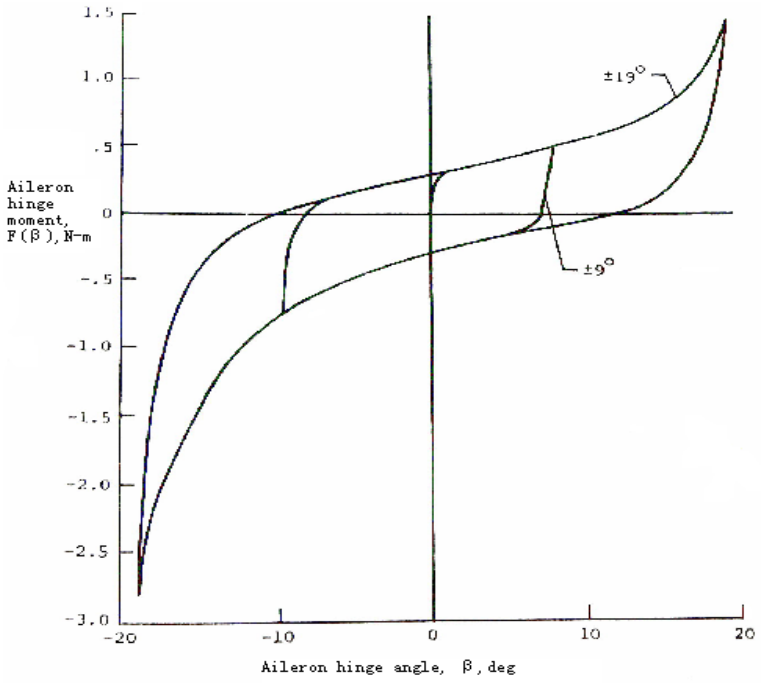

b)

Figure 1. Nonlinear force-deflection diagram of aileron system[22, 23].

Freeplay nonlinearity can be described by the following equation

$$f_f(x)=\begin{cases} x+\delta & x<-\delta \\ 0 & -\delta \le x \le \delta \\ x-\delta & x>\delta \end{cases} \tag{1}$$

When the freeplay $\delta = 0.25^\circ$, $f_f(x)$ can be fitted as the following rational polynomial

$$\overline{f}_f(x)=\frac{0.00002747-0.01702x-11.94x^2+5462x^3}{0.4556-12.36x+5732x^2} \tag{2}$$

The hysteresis nonlinearity has mathematic description as

$$f_h(x)=\begin{cases} x-x_f+F_0 & x<x_f,\uparrow \\ F_0 & x_f \le x \le x_f+\delta,\uparrow \\ x-x_f-\delta+F_0 & x>x_f+\delta,\uparrow \\ x+x_f-F_0 & x>-x_f,\downarrow \\ -F_0 & -x_f-\delta \le x \le -x_f,\downarrow \\ x+x_f+\delta-F_0 & x<-x_f-\delta,\downarrow \end{cases} \tag{3}$$

The parameters in Eq. (3) are defined in Fig. 2.

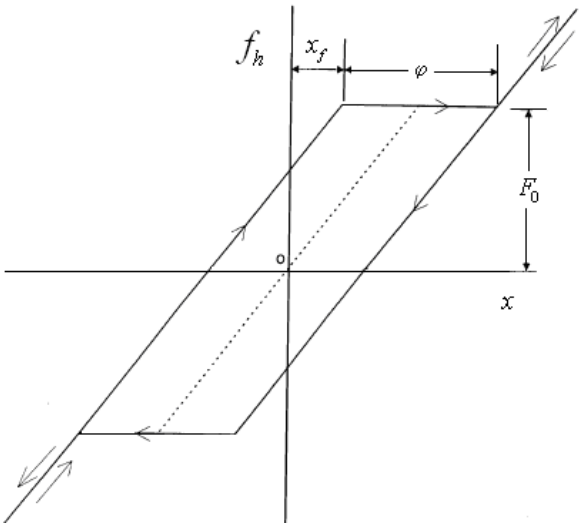

Figure2. Sketch of hysteresis nonlinearity.

When the nonlinear parameter in Eq. (3) $\varphi = 1.0^\circ$, $F_0 = 1.0^\circ$, and $x_f = 0.5^\circ$, $f_h(x)$ can be approximated as the following rational polynomial

$$\overline{f}_h(x)=\frac{0.935x^3-0.03073\psi x^2+0.0002284x+0.000005509\psi}{x^2-0.03382\psi x+0.0005796} \tag{4}$$

where, ψ is the velocity index,

$$\psi = sign(\dot{x})\cdot 1 \tag{5}$$

From Fig. 3, we can see that the rational polynomial in Eq. (2) and (4) give accurate approximation for both freeplay and hysteresis separately.

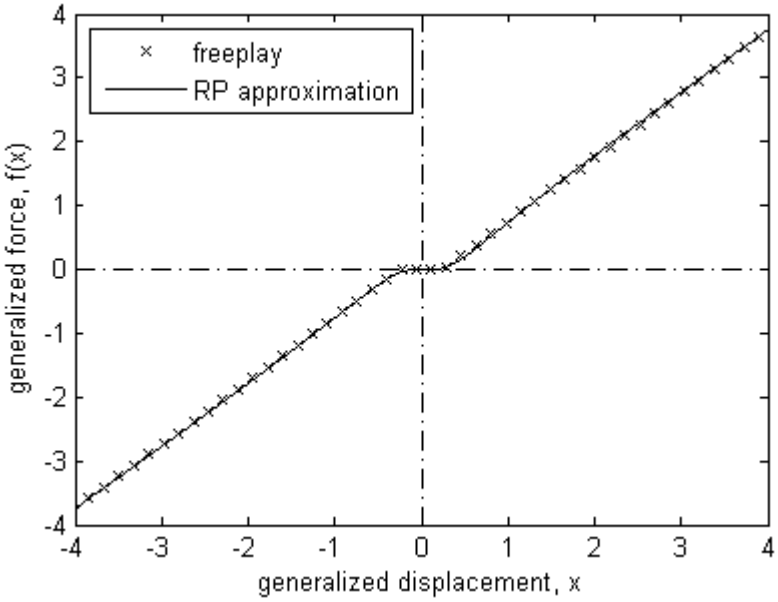

a)

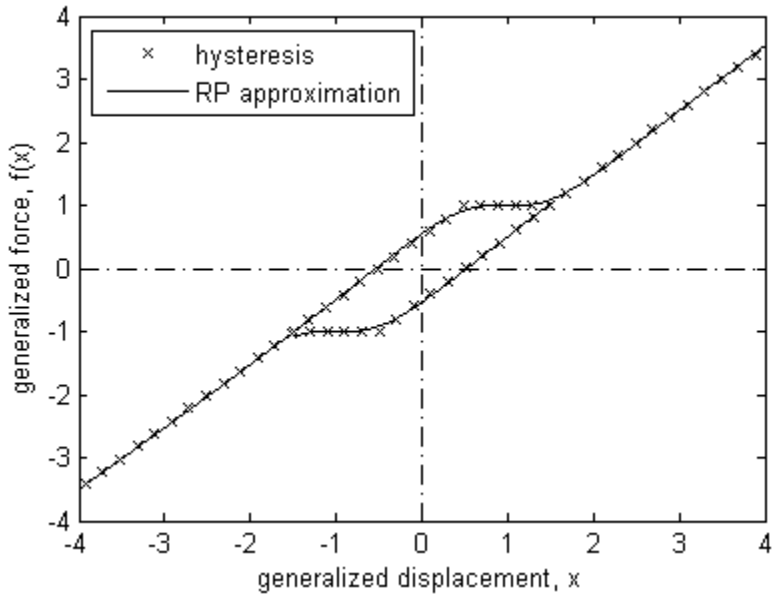

b)

Figure 3. Rational polynomial approximation of a): freeplay; and b): hysteresis.

In order to further verify that the RP nonlinearity model can describe freeplay or hysteresis in dynamic situation, we set RP model into pitching DOF of the aeroelastic airfoil described in Ref. 3. The dynamic equation was solved by using common Runge-Kutta numerical method. On the other hand, for freeplay or hysteresis nonlinearity in control surface, a key problem in numerical integration process is to locate the switching point at which the system moves from one sub domain into the next. Numerical instability may occur unless the switching points are located accurately. Based on the work done by Henon [24] and Conner et al. [25], the Henon's method is used to solve the integration problem with freeplay and hysteresis nonlinearity. The system parameters are chosen as: $a = -0.5$, $r = 0.5$, $d = 0.25$,

$\mu = 100$, and $\bar{\omega} = 0.2$. With the flow velocity U = 5.0*m/s*, aeroelastic responses of the system with freeplay or corresponding RP approximation are shown in Fig. 4, which indicate that the RP model agrees well with the original freeplay in the point of dynamic response. The similar results are obtained for the hysteresis and corresponding RP approximation, as shown in Fig. 5.

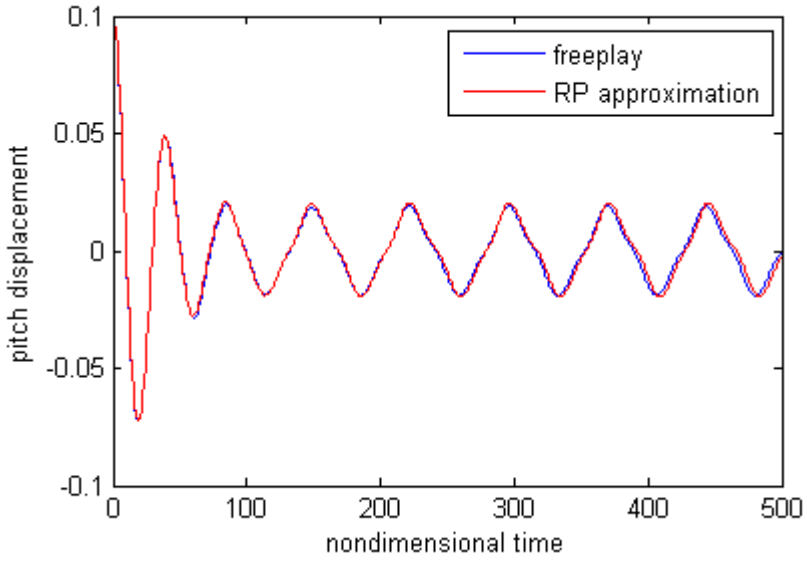

a)

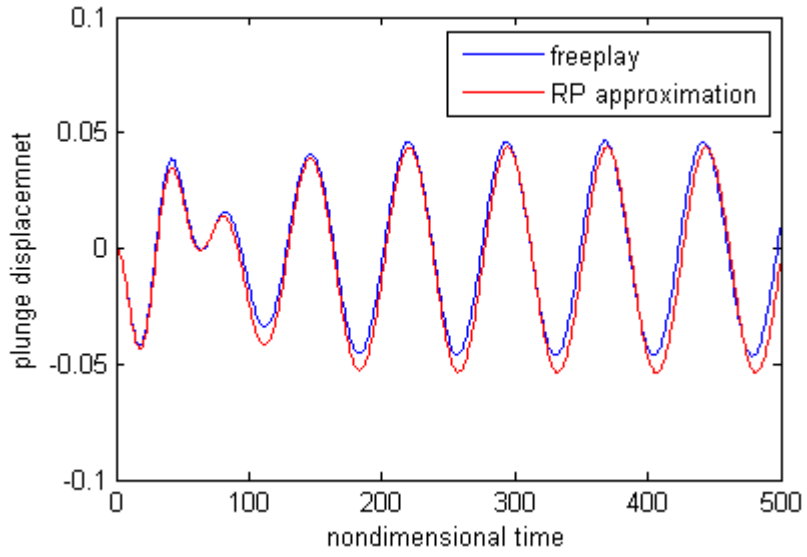

b)

Figure 4. Time histories of aeroelastic system with freeplay nonlinearity.

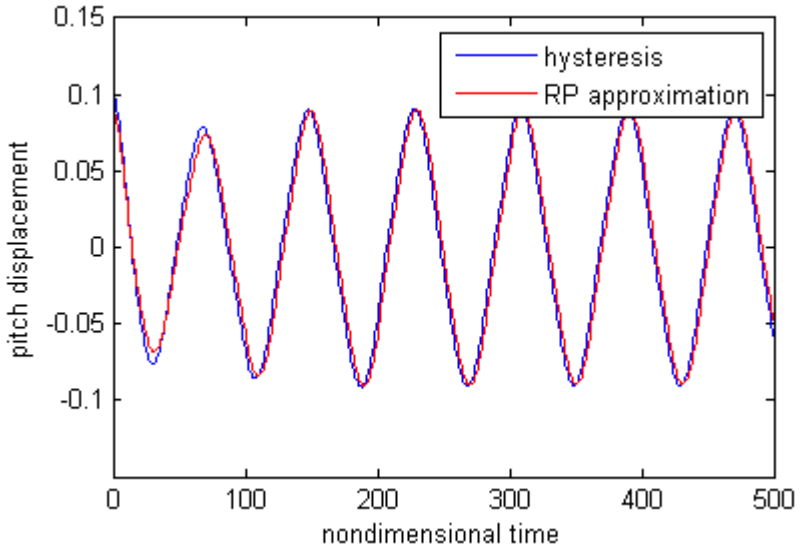

a)

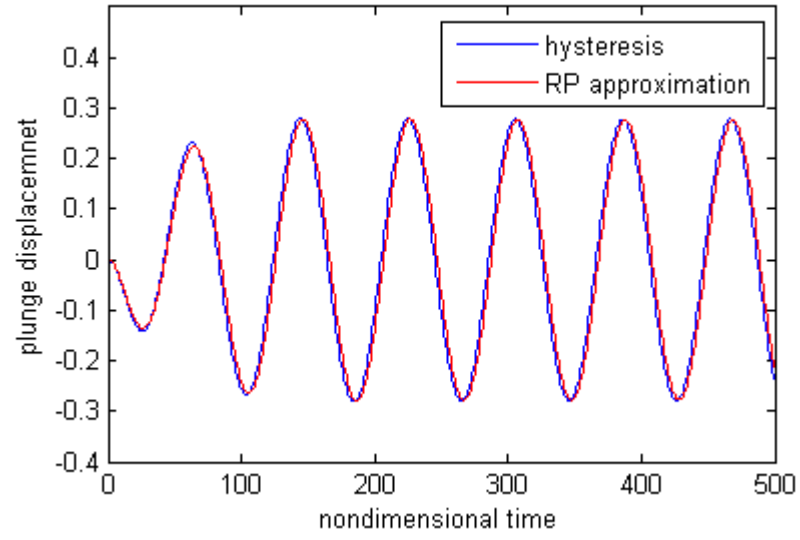

b)

Figure 5. Time histories of aeroelastic system with hysteresis nonlinearity.

III. Equations of Motion and Control Problem

In this section, we will apply the RP nonlinear model built in to describe the nonlinearity in control surface. So we can investigate the effect of nonlinearity on control performance. A typical airfoil section with a trailing edge control surface is normally simplified and modelled as a three degrees-of-freedom system as illustrated in Fig. 6 for aeroelastic analysis [19]. The three degrees of freedom of the model include plunge h, pitch α, and control surface angle β. The elastic axis is located at a distance ab from the mid-chord. The airfoil mass center is located at a distance $x_\alpha b$ from the elastic axis, where b is the semi-chord of the airfoil section. Both distances are positive when measured towards the airfoil trailing edge. There is a distance cb from the hinge line of the control surface, and a distance $x_\beta b$ from the mass center of the control surface to the mid-chord.

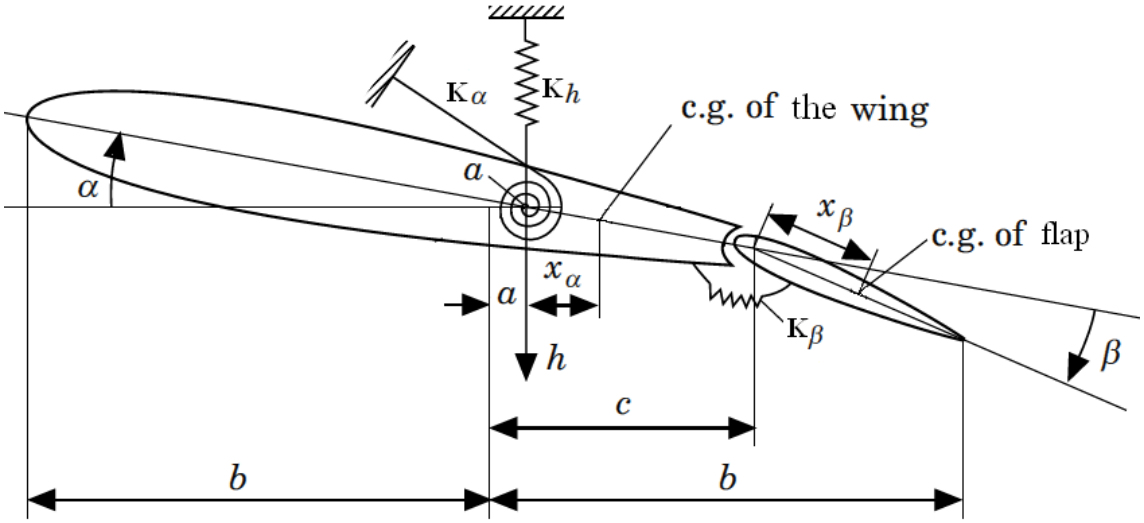

Figure 6. Schematic of airfoil section with a control surface.

The non-dimensional governing equations of motion for the airfoil aeroelastic model are given by

$$\begin{aligned} r_\alpha^{\,2}\ddot{\alpha} + \left[r_\beta^{\,2} + (c-a)x_\beta\right]\ddot{\beta} + x_\alpha\ddot{h} + r_\alpha^{\,2}\omega_\alpha^{\,2}\alpha &= M_\alpha/(mb^2) \\ \left[r_\beta^{\,2} + (c-a)x_\beta\right]\ddot{\alpha} + r_\beta^{\,2}\ddot{\beta} + x_\beta\ddot{h} + r_\beta^{\,2}\omega_\beta^{\,2}G(\beta) &= M_\beta/(mb^2) \\ x_\alpha\ddot{\alpha} + x_\beta\ddot{\beta} + (m_t/m)\ddot{h} + \omega_h^{\,2}h &= L/(mb) \end{aligned} \tag{6}$$

The parameters in Eq. (6) are defined in the nomenclature. The control surface moment rotation relationship $G(\beta)$ considering RP nonlinearity in the control surface is expressed as Eq. (2) or Eq. (4).

A structure damping matrix is created in this model according to Ref. 19 and Ref. 26. The eigenvalue λ_i, the natural frequency $\omega_i = \sqrt{\lambda_i}$, and eigenvector matrix $\mathbf{\Lambda}$ are determined from the left-hand side structure components of Eq. (6). Then the system modal mass matrix

$$\mathbf{M}_{mod} = \mathbf{\Lambda}^T\mathbf{M}_s\mathbf{\Lambda} \tag{7}$$

and the modal damping matrix B_{mod} can be obtained

$$\mathbf{B}_{mod} = \begin{bmatrix} 2m_\alpha\omega_\alpha\varsigma_\alpha & 0 & 0 \\ 0 & 2m_\beta\omega_\beta\varsigma_\beta & 0 \\ 0 & 0 & 2m_h\omega_h\varsigma_h \end{bmatrix} \tag{8}$$

where m_i are the values at the diagonal entries of $\mathbf{M}_{mod}$, and ς_i are the measured damping ratios. From the matrix $\mathbf{B}_{mod}$, the structure damping matrix can be obtained as $\mathbf{B}_s = \left(\mathbf{\Lambda}^{\mathbf{T}}\right)^{-1}\mathbf{B}_{mod}\left(\mathbf{\Lambda}\right)^{-1}$.

The unsteady aerodynamic force and moments in incompressible flow are given by[27]

$$
\begin{aligned}
M_\alpha &= -\rho b^2 \left\{ \pi (1/2 - a) U b \dot{\alpha} + \pi b^2 (1/8 + a^2) \ddot{\alpha} + (T_4 + T_{10}) U^2 \beta \right. \\
&+ \left[T_1 - T_8 - (c - a) T_4 + (1/2) T_{11} \right] U b \dot{\beta} - \left. \left[T_7 + (c - a) T_1 \right] b^2 \ddot{\beta} - a \pi b \ddot{h} \right\} \\
&+ 2 \rho U b^2 \pi (a + 1/2) C(k) \left[U \alpha + \dot{h} + b (1/2 - a) \dot{\alpha} + 1/\pi T_{10} U \beta + b (1/2\pi) T_{11} \dot{\beta} \right]
\end{aligned} \tag{9}
$$

$$
\begin{aligned}
M_\beta &= -\rho b^2 \left\{ \left[-2T_9 - T_1 + T_4 (a - 1/2) \right] U b \dot{\alpha} + 2 T_{13} b^2 \ddot{\alpha} \right. \\
&+ (1/\pi) U^2 \beta (T_5 - T_4 T_{10}) - (1/2\pi) U b \dot{\beta} T_4 T_{11} - \left. (1/\pi) T_3 b^2 \ddot{\beta} - T_1 b \ddot{h} \right\} \\
&\rho U b^2 T_{12} C(k) \left[U \alpha + \dot{h} + b (1/2 - a) \dot{\alpha} + 1/\pi T_{10} U \beta + b (1/2\pi) T_{11} \dot{\beta} \right]
\end{aligned} \tag{10}
$$

$$
\begin{aligned}
L &= -\rho b^2 (U \pi \dot{\alpha} + \pi \ddot{h} - \pi b a \ddot{\alpha} - U T_4 \dot{\beta} - T_1 b \ddot{\beta}) \\
&- 2 \pi \rho U b C(k) \left[U \alpha + \dot{h} + b (1/2 - a) \dot{\alpha} + 1/\pi T_{10} U \beta + b (1/2\pi) T_{11} \dot{\beta} \right]
\end{aligned} \tag{11}
$$

The Theodorsen constants T_i, i =1, 2,…13, are given in Appendix A. The aerodynamic force and moments in Eq. (9) –Eq. (11) are dependent on reduced frequency k. So Eq. (6) is restricted to simple harmonic oscillation.

Aerodynamics in Eq. (9) – Eq. (11) are dependent on Theodorsen's function, *C(k),* where k is the nondimensional reduced frequency of harmonic oscillation. So the aerodynamics is restricted to simple harmonic motion. In order to simulate arbitrary motion of the airfoil, Duhamel integral is used for the loading associated with *C(k).*

$$
L_c = C(k) f(t) = f(0) \phi(\tau) + \int_0^\tau \frac{\partial f(\sigma)}{\partial \sigma} \phi(\tau - \sigma) d\sigma \tag{12}
$$

where,

$$
f(t) = U \alpha + \dot{h} + b (1/2 - a) \dot{\alpha} + 1/\pi T_{10} U \beta + b (1/2\pi) T_{11} \dot{\beta} \tag{13}
$$

and $\phi(\tau)$ is Wagner function. In this paper, convenient approximation of Sears is used as

$$
\phi(\tau) \approx c_0 - c_1 e^{-c_2 \tau} - c_3 e^{-c_4 \tau} \tag{14}
$$

The coefficients in Eq. (14) are $c_1 = 0.165$, $c_2 = 0.0455$, $c_3 = 0.335$, and $c_4 = 0.3$.

In order to simplify the Theodorsen function, rewrite the Duhamel integral using integration by parts,

$$
L_c = f(\tau) \phi(0) + \int_0^\tau f(\sigma) \frac{\partial \phi(\tau - \sigma)}{\partial \sigma} d\sigma \tag{15}
$$

And Padé approximant method are used to represent the integral term as a second order ordinary differential equation as follow,

$$
L_c = (c_0 - c_1 - c_3) f(t) + c_2 c_4 (c_1 + c_3) \bar{x} + (c_1 c_2 + c_3 c_4) \dot{\bar{x}} \tag{16}
$$

After two augmented variables are introduced: $x_{a1} = \bar{x}$, $x_{a2} = \dot{\bar{x}}$, Eq. (1) can be expressed in a matrix form [28],

$$
(\mathbf{M}_s - \mathbf{M}_{NC}) \ddot{\mathbf{x}} + (\mathbf{B}_s - \mathbf{B}_{NC} - 1/2 \mathbf{R} \mathbf{S}_2) \dot{\mathbf{x}} + (\mathbf{K}_s - \mathbf{K}_{NC} - 1/2 \mathbf{R} \mathbf{S}_1) \mathbf{x} - \mathbf{R} \mathbf{S}_3 \mathbf{x}_a = 0 \tag{17}
$$

where $\mathbf{x} = \left[\alpha \quad \beta \quad h/b \right]^T$, and $\mathbf{x_a} = \left[x_{a1} \quad x_{a2} \right]^T$. Further details of the matrices and the additional vector terms

are given in Appendix B.

After introducing a variable vector $\mathbf{X}=\begin{bmatrix}\mathbf{x}^T & \dot{\mathbf{x}}^T & \mathbf{x}_a{}^T\end{bmatrix}^T$, $\mathbf{X}\in\mathbf{R}^8$, Eq. (13) can be rewritten in a state-space form

$$\dot{\mathbf{X}}=\mathbf{A}(\mathbf{X})\mathbf{X}+\mathbf{B}\beta_c \tag{18}$$

where β_c is the command input. The definition of matrix $\mathbf{A}(\mathbf{X})$ is given in Appendix C. Matrix **B** is given by

$$\mathbf{B}=\begin{bmatrix}0_{3\times1}\\ \mathbf{M}_t^{-1}\mathbf{G}\\ 0_{2\times1}\end{bmatrix} \tag{19}$$

where $\mathbf{G}=\begin{bmatrix}0 & r_\beta{}^2\omega_\beta{}^2 & 0\end{bmatrix}$.

IV. Control Law Design

In this section, a nonlinear flutter control law based on the state-dependent Riccati equation method [15-17] is designed. Consider the optimal infinite-horizon regulator problem, the performance index *J* is to be minimized subject to the system expressed by Eq. (18).

$$J=\frac{1}{2}\int_0^\infty\left(\mathbf{X}^T\mathbf{Q}(\mathbf{X})\mathbf{X}+r\beta_c{}^2\right)dt \tag{20}$$

where $\mathbf{Q}(\mathbf{X})$ is a positive definite symmetric matrix and $r>0$ for $\mathbf{X}\in\mathbf{R}^8$.

For the system modeled in Eq. (14), the controllability matrix is given by

$$\begin{bmatrix}\mathbf{B}, & \mathbf{A(X)B}, & \mathbf{A}^2\mathbf{(X)B}, & \cdots & \mathbf{A}^8\mathbf{(X)B}\end{bmatrix} \tag{21}$$

In order to obtain the suboptimal solution of the preceding problem, we solve the state-dependent Riccati equation given by

$$\mathbf{A}^T(\mathbf{X})\mathbf{P}(\mathbf{X})+\mathbf{P}(\mathbf{X})\mathbf{A}(\mathbf{X})-\mathbf{P}(\mathbf{X})\mathbf{B}\mathbf{R}^{-1}\mathbf{B}^T\mathbf{P}(\mathbf{X})+\mathbf{Q}(\mathbf{X})=0 \tag{22}$$

for a symmetric positive definite matrix $\mathbf{P}(\mathbf{X})$, the nonlinear feedback control law is given by

$$\beta_c(\mathbf{X})=-\mathbf{R}^{-1}\mathbf{B}^T\mathbf{P}(\mathbf{X})\mathbf{X} \tag{23}$$

Substituting Eq. (23) into Eq. (18), the closed-loop system is obtained as follow

$$\dot{\mathbf{X}}=\bar{\mathbf{A}}(\mathbf{X})\mathbf{X} \tag{24}$$

where the closed-loop system matrix is given by

$$\bar{\mathbf{A}}(\mathbf{X})=\mathbf{A}(\mathbf{X})-\mathbf{B}\mathbf{R}^{-1}\mathbf{B}^T\mathbf{P}(\mathbf{X}) \tag{25}$$

V. Results and Discussion

Nonlinear closed-loop control simulation results of aeroelastic system with RP nonlinearity in control surface are presented in this section. The values for the system parameters are taken from Ref. 19 and listed as follows: *a* = -0.5, *b*

= 0.127m, c = 0.5, s = 0.52m, m_T = 1.2895 kg, I_α = 0.01347 kg.m^2, I_β = 0.0003264 kg.m^2, x_α = 0.434, x_β = 0.01996, k_h = 2818.8 N/m, S_α = 0.08587 kg.m, S_β = 0.00395 kg.m, ρ = 1.225 kg/m^3, $\varsigma_1 = 0.01626$, $\varsigma_2 = 0.0115$, $\varsigma_3 = 0.0113$. The aeroelastic system described in Eq. (25) was solved by using Runge-Kutta numerical integration, and the time step was set as 0.001s.

5.1 Closed-loop response with RP freeplay

If β_c = 0, then the system Eq. (25) becomes open-loop. When there is not any nonlinearity exists in the control surface, Now the system response keeps stable until the velocity reaches up to U = 23.96 m/s. However, the system with RP freeplay exhibits obvious limit cycle oscillation at a quite low velocity (about U = 6.0 m/s), which is relative to the initial conditions used in the simulation.

In the following closed-loop situation, state coefficient matrix **Q** in performance index is chose as a 8*8 unit matrix, and control input coefficient r = 100. First the simulation is run with the flow velocity of U = 24.0 m/s, which is above both linear and RP freeplay flutter speed. Figure 7 shows the closed-loop pitch, flap, and plunge histories. We observe that there is no obvious difference between linear and RP freeplay system responses when the time t < 1s. However, the linear responses converge to zero point whereas the RP freeplay responses converge to nonzero constant, especially flap and plunge states. It is found that the flap variable of RP freeplay system converges to half of the freeplay (0.25 deg or 0.0044 rad), which is shown as dashed line in Fig. 7. b.

a)

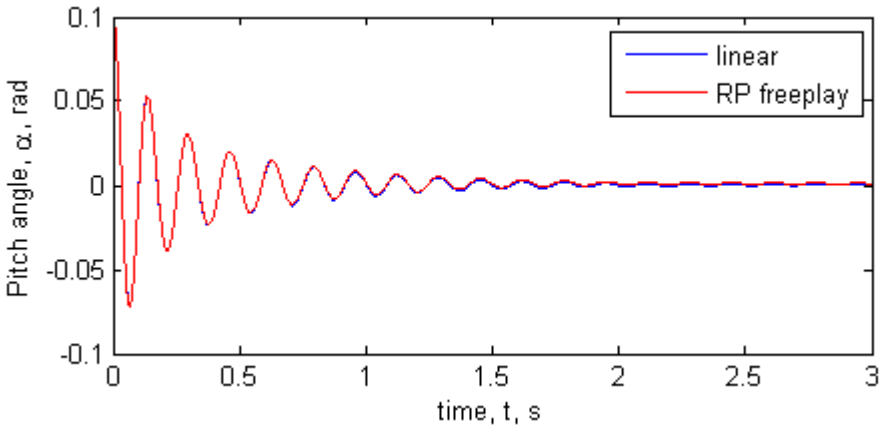

b)

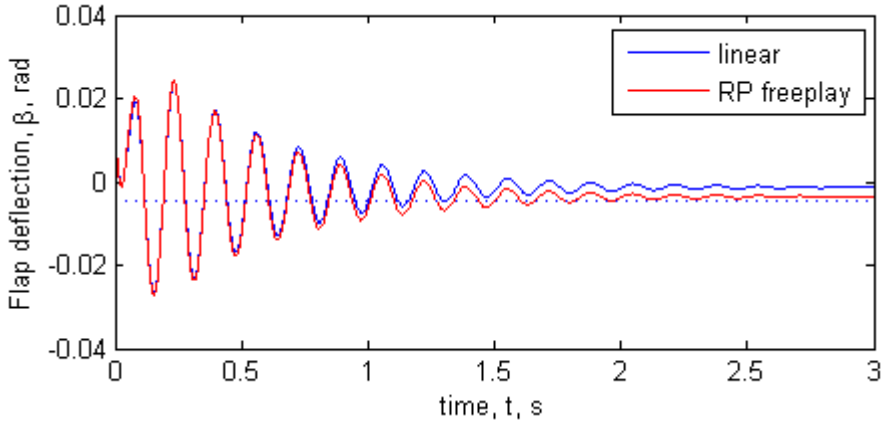

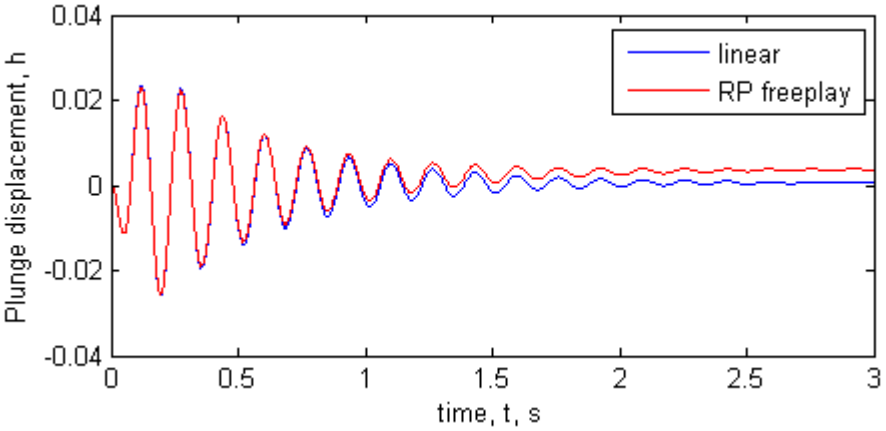

c)

Figure 7. Flutter suppression with and without RP freeplay at *U* = 24.0 m/s: a) pitch; b) flap; c) plunge.

For a higher flow velocity (*U* = 30.0 m/s), the simulation is performed, as shown in Fig. 8. It is noted that a faster response time of less than 1.0 second is obtained. And the maximum control magnitude (-0.12 rad) is larger than the maximum in Fig.7.b (-0.03 rad). Both pitch and flap time histories of RP freeplay system converge to nonzero constants, while plunge time history looks more like linear plunge time history (Fig.8.c).

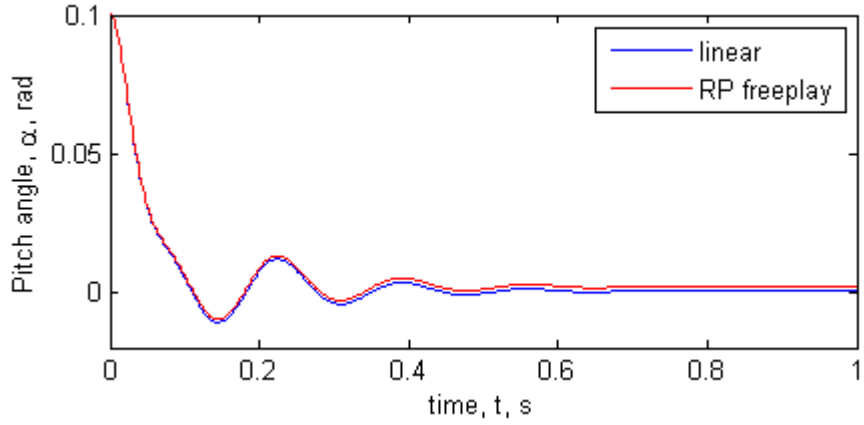

a)

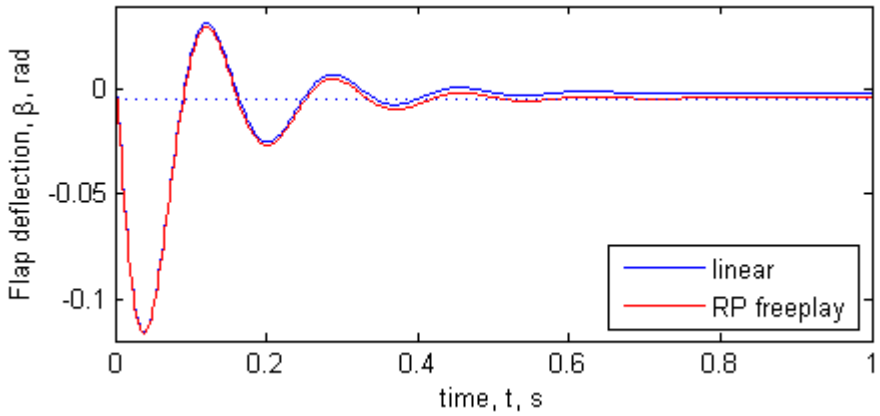

b)

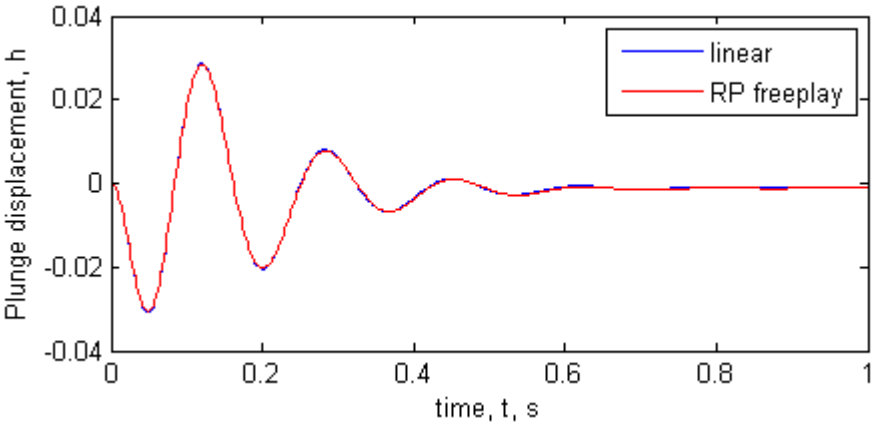

c)

Figure 8. Flutter suppression with and without RP freeplay at U = 30.0 m/s: a) pitch; b) flap; c) plunge.

5.2 Closed-loop system response with RP hysteresis

For the aeroelastic system with RP hysteresis nonlinearity, the simulation was first performed with the flow velocity U = 24.0 m/s, which is above RP hysteresis critical flutter speed. As shown in Fig. 9, both pitch and plunge responses of the RP hysteresis system take much longer time than linear system responses to converge to zero points. However, at a higher flow velocity U = 30.0 m/s, there is no obvious difference between the linear and RP hysteresis system responses. And a faster response time of less than one second was obtained and shown in Fig. 10.

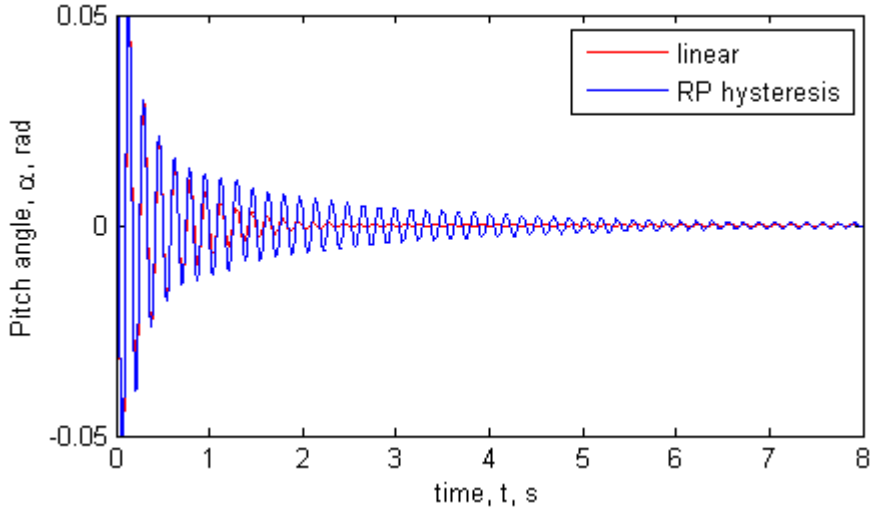

a)

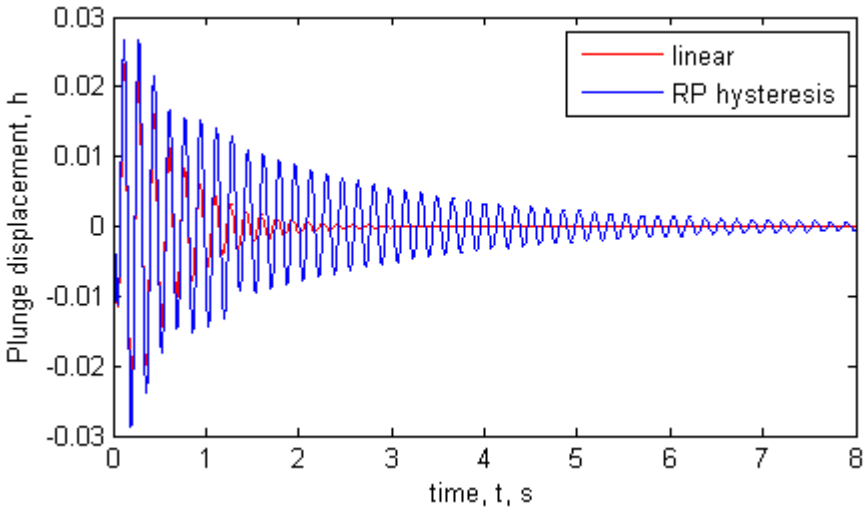

b)

Figure 9. Flutter suppression with and without RP hysteresis at *U* = 24.0 m/s: a) pitch; plunge.

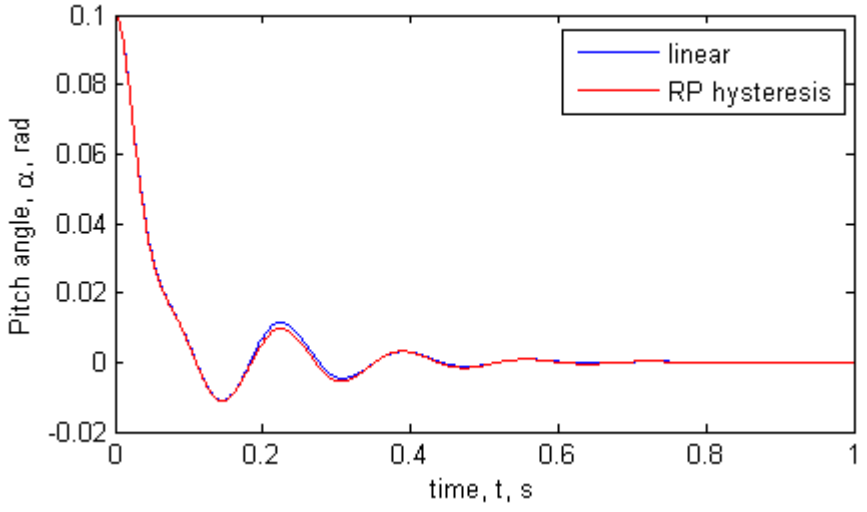

a)

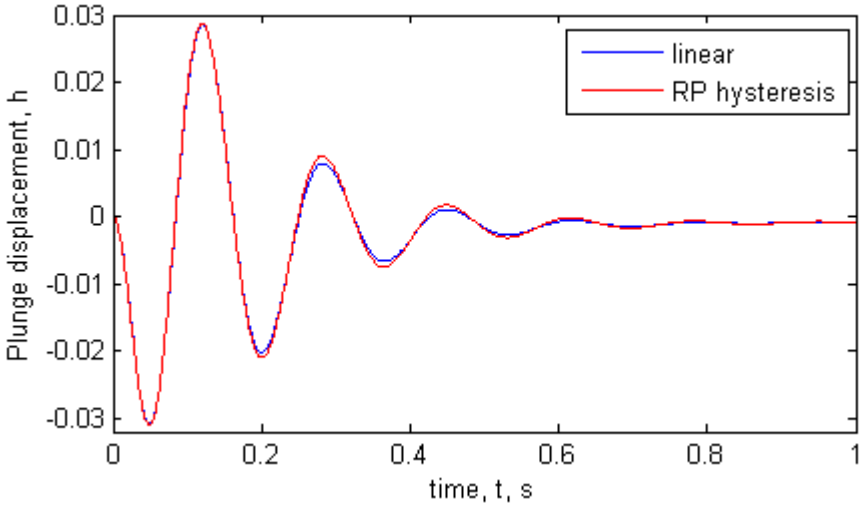

b)

Figure 10. Flutter suppression with and without RP hysteresis at *U* = 30.0 m/s: a) pitch; b) plunge.

VI. Conclusions

In this paper, a rational polynomial approximation model is introduced based on actual measured force-deflection relation in aileron system. The model can be used to describe all the three classical nonlinearities in aeroelastic system: cubic, freeplay, and hysteresis, which was verified by numerical example. The aeroelastic system with RP nonlinearity is differentiable, so the switching point problem can be avoided in the numerical integration process.

Then a state space dynamic equation of a three degree of freedom aeroelastic airfoil with the RP nonlinearity in control surface was derived. And a state feedback suboptimal control law for flutter suppression of the typical airfoil section was designed with state-dependent Riccati equation method. With the control law designed in this paper, the effects of both RP freeplay and hysteresis on the aeroelastic responses have been investigated. The aeroelastic response of system with RP freeplay does not converge to zero points. And the RP hysteresis system responses take a much longer time to converge than linear responses.

Appendix

Appendix A: Theodorsen Constants in Eq. (9) - Eq. (11)

$$T_1 = -1/3\sqrt{1-c^2}\left(2+c^2\right)+\cos^{-1}c$$

$$T_3 = -(1/8)c\left(1-c^2\right)\left(5c^2+4\right)+1/4\left(7+2c^2\right)\sqrt{1-c^2}\cos^{-1}c-\left(1/8+c^2\right)\left(\cos^{-1}c\right)^2$$

$$T_4 = c\sqrt{1-c^2}-\cos^{-1}c$$

$$T_5 = -\left(1-c^2\right)+2c\sqrt{1-c^2}\cos^{-1}c-\left(\cos^{-1}c\right)^2$$

$$T_7 = (1/8)c\left(7+2c^2\right)-\left(1/8+c^2\right)\cos^{-1}c$$

$$T_8 = -(1/3)\left(1+2c^2\right)\sqrt{1-c^2}+c\cos^{-1}c$$

$$T_9 = 1/2\left[1/3\left(\sqrt{1-c^2}\right)^3+aT_4\right]$$

$$T_{10} = \sqrt{1-c^2}+\cos^{-1}c$$

$$T_{11} = \left(\cos^{-1}c\right)(1-2c)+\sqrt{1-c^2}\left(2-c\right)$$

$$T_{12} = \sqrt{1-c^2}\left(2+c\right)-\left(\cos^{-1}c\right)(2c+1)$$

$$T_{13} = 1/2\left[-T_7-(c-a)T_1\right]$$

Appendix B: Definitions of Matrices Appearing in Eq. (17)

$$\mathbf{M_s} = \begin{bmatrix} r_\alpha^{\,2} & r_\beta^{\,2} + (c-a)x_\beta & x_\alpha \\ r_\beta^{\,2} + (c-a)x_\beta & r_\beta^{\,2} & x_\beta \\ x_\alpha & x_\beta & M_t / M \end{bmatrix}$$

$$\mathbf{B_s} = \left(\mathbf{\Lambda}^T\right)^{-1} \begin{bmatrix} 2m_\alpha \omega_\alpha \varsigma_\alpha & 0 & 0 \\ 0 & 2m_\beta \omega_\beta \varsigma_\beta & 0 \\ 0 & 0 & 2m_h \omega_h \varsigma_h \end{bmatrix} \mathbf{\Lambda}^{-1}$$

$$\mathbf{K_s} = \begin{bmatrix} r_\alpha^{\,2} \omega_\alpha^{\,2} F(\alpha)/\alpha & 0 & 0 \\ 0 & r_\beta^{\,2} \omega_\beta^{\,2} G(\beta)/\beta & 0 \\ 0 & 0 & \omega_h^{\,2} \end{bmatrix}$$

$$\mathbf{M_{NC}} = -\frac{\rho}{m} \begin{bmatrix} \pi b^2 (1/8 + a^2) & -(T_7 + (c-a)T_1) b^2 & -\pi a b^2 \\ 2T_{13} b^2 & -T_3 b^2/\pi & -T_1 b^2 \\ -\pi a b^2 & -T_1 b^2 & \pi b^2 \end{bmatrix}$$

$$\mathbf{B_{NC}} = -\frac{\rho}{m} \begin{bmatrix} \pi(1/2 - a) Ub & \left(T_1 - T_8 - (c-a)T_4 + T_{11}/2\right) Ub & 0 \\ \left(-2T_9 - T_1 + T_4(a - 1/2)\right) Ub & -T_4 T_{11} Ub/(2\pi) & 0 \\ \pi Ub & -UT_4 b & 0 \end{bmatrix}$$

$$\mathbf{K_{NC}} = -\frac{\rho}{m} \begin{bmatrix} 0 & (T_4 + T_{10}) U^2 & 0 \\ 0 & (T_5 - T_4 T_{10}) U^2/\pi & 0 \\ 0 & 0 & 0 \end{bmatrix}$$

$$\mathbf{R} = \begin{bmatrix} 2\pi\rho U(a + 1/2)/m & -\rho U T_{12}/m & -2\pi\rho U/m \end{bmatrix}^T$$

$$\mathbf{S}_1 = \begin{bmatrix} U & T_{10} U/\pi & 0 \end{bmatrix}$$

$$\mathbf{S}_2 = \begin{bmatrix} b(1/2 - a) & bT_{11}/2\pi & b \end{bmatrix}$$

$$\mathbf{S}_3 = \begin{bmatrix} c_2 c_4 (c_1 + c_3) U^2/b & (c_1 c_2 + c_3 c_4) U \end{bmatrix}.$$

Appendix C: Definitions of Matrices Appearing in Eq. (18)

$$\mathbf{A} = \begin{bmatrix} 0 & \mathbf{I}_{3\times 3} & 0 \\ -\mathbf{M_t}^{-1}\mathbf{K_t} & -\mathbf{M_t}^{-1}\mathbf{B_t} & \mathbf{M_t}^{-1}\mathbf{D} \\ \mathbf{E}_1 & \mathbf{E}_2 & \mathbf{F} \end{bmatrix},$$

where, $\mathbf{M_t} = \mathbf{M_s} - \mathbf{M_{NC}}$, $\mathbf{B_t} = \mathbf{B_s} - \mathbf{B_{NC}} - 1/2\mathbf{RS}_2$, $\mathbf{K_t} = \mathbf{K_s} - \mathbf{K_{NC}} - 1/2\mathbf{RS}_1$, $\mathbf{D} = \mathbf{RS}_3$,

$$\mathbf{E}_1 = \begin{bmatrix} 0 & 0 & 0 \\ U/b & UT_{10}/(\pi b) & 0 \end{bmatrix},\ \mathbf{E}_2 = \begin{bmatrix} 0 & 0 & 0 \\ (1/2-a) & T_{11}/(2\pi) & 1 \end{bmatrix},\ \mathbf{F} = \begin{bmatrix} 0 & 1 \\ -c_2c_4U^2/b & -(c_2+c_4)U/b \end{bmatrix}.$$

Acknowledgments

The authors would like to acknowledge the EC funding for the EU FP7 collaborative project SADE and the National Nature Science Grant of P.R. China (No. 90916006).

References

[1] Lee, B. H. K., Price, S. J., and Wong, Y. S., "Nonlinear Aeroelastic Analysis of Airfoil: Bifurcation and Chaos," *Progress in Aerospace Science*, Vol. 35, No. 3, 1999, pp. 205-334.

[2] Dowell, E. H., Edwards, J., and Strganac, T., "Nonlinear Aeroelasticity," *Journal of Aircraft*, Vol. 40, No. 5, 2003, pp. 857-874.

[3] Li, D., and Xiang, J., "Chaotic Motions of an Airfoil with Cubic Nonlinearity in Subsonic Flow," *Journal of Aircraft*, Vol. 45, No. 4, 2008, pp. 1457-1460.

[4] Kurdila, A. J., Strganac, T. W., Junkins, J. L., Ko, J., and Akella, M. R., "Nonlinear control methods for high-energy limit-cycle oscillations," *Journal of Guidance, Control, and Dynamics*, Vol. 24, No. 1, 2001, pp. 185-192.

[5] Mukhopadhyay, V., "Historical Perspective on Analysis and Control of Aeroelastic Responses," *Journal of Guidance, Control, and Dynamics*, Vol. 26, No. 5, 2003, pp. 673-684.

[6] Lin, C. M., and Chin, W. L., "Adaptive Decoupled Fuzzy Sliding-Model Control of a Nonlinear Aeroelastic System," *Journal of Guidance, Control, and Dynamics*, Vol. 29, No. 1, 2006, pp. 206-209.

[7] Baranyi, P., "Tensor-Product Model-Based Control of Two-Dimensional Aeroelastic System," *Journal of Guidance, Control, and Dynamics*, Vol. 29, No. 2, 2006, pp. 391-400.

[8] Baranyi, P., "Out feedback control of two-dimensional aeroelastic system," *Journal of Guidance, Control, and Dynamics*, Vol. 29, No. 3, 2006, pp. 762-767.

[9] Bihal, A., Rao, V. M., and Marzocca, P., "Adaptive Control for a Nonlinear Wing Section with Multiple Flaps," *Journal of Guidance, Control, and Dynamics*, Vol. 29, No. 5, 2006, pp. 744-748.

[10] Singh, S. N., Wang, L., "Output feedback form and adaptive stabilization of a nonlinear aeroelastic system," *Journal of Guidance, Control, and Dynamics*, Vol. 25, No. 5, 2002, pp. 725-732.

[11] Singh, S. N., Brenner, M., "Modular adaptive control of a nonlinear aeroelastic system," *Journal of Guidance, Control, and Dynamics*, Vol. 26, No. 3, 2003, pp. 443-451.

[12] Xing, W., Singh, S. N., "Adaptive output feedback control of a nonlinear aeroelastic structure," *Journal of Guidance, Control, and Dynamics*, Vol. 23, No. 6, 2000, pp. 1109-1136.

[13] Zhang, R., Singh, S. N., "Adaptive output feedback control of an aeroelastic system with unstructured uncertainties," *Journal of Guidance, Control, and Dynamics*, Vol. 24, No. 3, 2001, pp. 502-509.

[14] Lee, K. W., Singh, S. N., "Global robust control of an aeroelastic system using output feedback," *Journal of Guidance, Control, and Dynamics*, Vol. 30, No. 1, 2007, pp. 271-275.

[15] Mracek, C. P., and Cloutier, J. R., "Control Designs for the Nonlinear Benchmark Problem via the State-Dependent Riccati Equation Method," *International Journal of Robust and Nonlinear Control*, Vol. 8, No. 4-5, 1998, pp. 401-433.

[16] Tadi, M., "State-Dependent Riccati Equation for Control of Aeroelastic Flutter," *Journal of Guidance, Control, and Dynamics*, Vol. 26, No. 6, 2003, pp. 914-917.

[17] Bhoir, N., and Singh, S. N., "Control of Unsteady Aeroelastic System via State-Dependent Riccati Equation Method," *Journal of Guidance, Control, and Dynamics*, Vol. 28, No. 1, 2005, pp. 78-84.

[18] Edwards, J. W., Ashley H., and Breakwell, J. V., "Unsteady Aerodynamic Modeling for Arbitrary Motions," *AIAA Journal*, Vol. 17, No. 4, 1979, pp. 365-374.

[19] Conner, M. D., Tang, D. M., Dowell, E. H., and Virgin, L. N., "Nonlinear Behavior of a Typical Airfoil Section with Control Surface Freeplay: a Numerical and Experimental Study," *Journal of Fluids and structures*, Vol. 11, 1997, pp. 89-109.

[20] Woolston D. S., Runyan H. L., Byrdsong T. A.. "Some Effects of System Nonlinearities in the Problem of Aircraft Flutter". NACA-TN-3539, 1955.

[21] Woolston D. S., Runyan H. L., Andrews R. E.. "An Investigation of Certain Types of Structural Nonlinearities on Wing and Control Surface Flutter". *Journal of the Aeronautical Sciences*, Vol. 24, No. 1, 1957, pp: 57-63.

[22] Breitbach E. J., "Effect of Structural Nonlinearities on Aircraft Vibration and Flutter," AGADD-R-665, 1977.

[23] Breitbach E. J., "Flutter Analysis of an Airplane with Multiple Structural Nonlinearities in the Control System," NASA-TP-1620, 1980.

[24] Henon, M., "On the Numerical Computation of Poincaré Map," Physica D, Vol. 5, 1982, pp. 412-414.

[25] Conner, M. D., Virgin, L. N., and Dowell E. H., "Accurate Numerical Integration of State-Space Models for Aeroelastic Systems with Free Play," *AIAA Journal*, Vol. 34, No. 10, 1996, pp. 2202-2205.

[26] Liu, L., and Dowell, E. H., "Harmonic Balance Approach for an Airfoil with a Freeplay Control Surface," *AIAA Journal*, Vol. 43, No. 4, 2005, pp. 802-815.

[27] Theodorsen, T., "General Theory of Aerodynamic Instability and the Mechanism of Flutter," NACA Report 496, 1935.

[28] Trickey, S. T., "Global and Local Dynamics of an Aeroelastic System with a Control Surface Freeplay Nonlinearity," Ph.D. Dissertation, Department of Mechanical Engineering and Material Science, Duke University, Durham, NC, 2000.